

Combining Machine Learning and Spectroscopy to Model Reactive Atom + Diatom Collisions

Juan Carlos San Vicente Veliz,[†] Julian Arnold,[‡] Raymond J. Bemish,[¶] and Markus Meuwly^{*,†}

[†]*Department of Chemistry, University of Basel, Klingelbergstrasse 80, CH-4056 Basel, Switzerland*

[‡]*Department of Physics, University of Basel, Klingelbergstrasse 82, CH-4056 Basel, Switzerland*

[¶]*Air Force Research Laboratory, Space Vehicles Directorate, Kirtland AFB, New Mexico 87117, USA*

E-mail: m.meuwly@unibas.ch

September 2, 2022

Abstract

The prediction of product translational, vibrational, and rotational energy distributions for arbitrary initial conditions for reactive atom+diatom collisions is of considerable practical interest in atmospheric re-entry. Due to the large number of accessible states, determination of the necessary information from explicit (quasi-classical or quantum) dynamics studies is impractical. Here, a machine-learned (ML) model based on translational energy and product vibrational states assigned from a spectroscopic, rovibrational coupled energy expression based on the Dunham expansion is developed and

tested quantitatively. All models considered in this work reproduce final state distributions determined from quasi-classical trajectory (QCT) simulations with $R^2 \sim 0.98$. As a further validation, thermal rates determined from the machine-learned models agree with those from explicit QCT simulations and demonstrate that the atomistic details are retained by the machine learning which makes them suitable for applications in more coarse-grained simulations. More generally, it is found that ML is suitable for designing robust and accurate models from mixed computational/experimental data which may also be of interest in other areas of the physical sciences.

Introduction

Atom-diatom collisions at high collision energy are complex due to the multitude of possible ways in which the available energy can be redistributed. Relevant processes include reactions, exchange of energy into translation, rotation, and vibration and depending on the energy, low-lying electronic states. The number of possible states that are accessible increases exponentially with the available energy. To be able to understand bulk energy transfer in high-energy processes, the probabilities of these processes need to be quantified and understood.

For a reactive atom-diatom collision, determining all state-to-state cross sections is computationally very challenging even when treating the process within classical mechanics. This is due to the large number of reactant states ($\sim 10^4$) that can combine with any product state (also $\sim 10^4$) which gives rise to $\sim 10^8$ state-to-state cross sections. If such cross sections are determined from quasi-classical trajectory (QCT) simulations, typically 10^4 to 10^5 simulations are required for converged results which yields an estimated 10^{12} to 10^{13} QCT simulations that would have to be run at a given collision energy. Depending on the range of relevant collision energies (~ 5 eV in hypersonics) the number of required QCT simulations can further increase by one or two orders of magnitude. This is usually not possible nor desir-

able. With individual QCT calculations taking roughly one second, even parallelization and Moore's law scaling for improvement in processor speed will not provide sufficient speedup for exhaustive calculations in the next decades. Current computer technology limits tractable calculations to 10^8 meaning that any complete model for the probabilities determined from QCT simulations would be supported by one in $\sim 10^7$ outcomes. In other words: either many final state distributions are unconverged or the final states are not covered at all, or both. This sparse representation creates a challenge for accurately modeling the molecular dynamics in a way that is useful to larger scale simulations. However, because state-to-state cross sections are of paramount importance to determine rates for the process of interest, alternative ways to address the problem are required as this information is further used in reaction networks to model more complicated chemistries.

One application for which this is particularly relevant, is the high temperature, high enthalpy flow prevalent in hypersonics. It is not uncommon to find nominal temperatures that exceed 10000 K in shocks and expansions that cause local non-equilibrium in the rovibrational states of the chemically active molecules. Following the dynamics and chemical development of rarefied gas flows employs primarily two strategies. One uses computational fluid dynamics (CFD)¹ which is based on the Navier Stokes formulation of fluid dynamics and is valid for small Knudsen number (ratio of the mean free path length to a physical length scale), whereas direct simulation Monte Carlo (DSMC)² is more broadly applicable and is also valid for high Knudsen number. In DSMC, particles (representing the physical atoms and molecules) move and collide in physical space to which techniques from statistical mechanics can be applied.³ Particles in DSMC carry information about their position, velocity, mass, size, and internal state (for molecules) and move in cells within which they can collide and exchange energy.

DSMC cycles through the following steps: 1.) moving particles over a time step Δt smaller

than the local mean free collision time; 2.) moving particles across cell boundaries or reflecting them at solid boundaries; 3.) changing their internal states as a consequence of collisions or reactions; 4.) sample average particle information.³ Step 3 is where microscopic information about thermal reaction rates, state-to-state cross sections, and vibrational relaxation rates enters. For chemical reactions most often the “total collision model”, based on a modified Arrhenius equation, is used,⁴ although more refined models are also available.⁵ A more detailed and accurate description is afforded by state-to-state or state-to-distribution models. However, experimentally, it is very challenging or even impossible to determine the relevant quantities at sufficiently high temperature. Most cross sections presently used are derived from chemical kinetics, many of which have not been measured at and above 3000 K, or can not be measured but are required at even higher temperatures. Alternatively, the essential information can also be obtained from quasi-classical trajectory (QCT) simulations using state-of-the-art potential energy surfaces. Such an approach provides all necessary information but implicitly assumes that the PESs and the classical dynamics underlying QCT simulations are meaningful. In the present work information from experimental spectroscopy is blended into such a model.

A widely used model for describing microscopic details of hypersonic flow including chemical and relaxation processes is due to Park.^{6,7} This approach considers separate temperatures T_v and T_t for the vibration and rotation/translation, respectively. In application to kinetics the temperature is taken to be the geometric mean of these, the so-called “ $T - T_v$ model”. “Chemistry” enters such models through forward and reverse reaction rates in the law of mass action for interacting chemical species which are often determined from temperature-dependent (modified) Arrhenius expressions. Following and extending the approach from Millikan and White,⁸ an important intuitive correction established a framework for including vibrational non-equilibrium in vibrational relaxation.⁹

One problematic aspect of the Park model is that vibrational energy becomes “frozen” above the translational energy because vibrational relaxation is only included within the limits of Landau-Teller theory^{8,10,11} but the contribution that accounts for removal of vibrational energy due to dissociation of the product is neglected as is the movement of large amounts of translational energy to vibrational energy via atom exchange reactions. Including the contribution arising from dissociation of the diatomic products was addressed and corrected in a recent kinetic model which, however, neglected explicit coupling between intramolecular rotation and vibration.^{12,13} Also, with larger computational platforms, it has been possible to investigate the underlying physics on which the Park approach rests, namely the two-temperature assumption and the preferential dissociation model¹⁴ which assumes that the amount of vibrational energy removed during dissociation is large. For $\text{N}_2 + \text{N}$ and $\text{N}_2 + \text{N}_2$ it was shown that the $T - T_v$ model predicts a much faster N_2 dissociation for $T \leq 20000$ K than that obtained with direct molecular simulation (DMS) whereas for $T = 30000$ K the two models agree.¹⁵

Machine-learned (ML) models have proven to be effective in predicting product distributions based on information about initial states (E_{trans}, v, j) . For one, a neural network (NN) based state-to-state (STS) model was conceived that predicts the cross section for a given transition $(E_{\text{trans}}, v, j) \rightarrow (E'_{\text{trans}}, v', j')$. This was demonstrated for the [NNO] reactive system¹⁶ in that not only the cross sections for transitions that were not part of the training set were correctly predicted, but also quantities derived from the cross sections – such as the total thermal rate $k(T)$ – are in very good agreement with those determined directly from QCT simulations. Conversely, a distribution-to-distribution (DTD) model is capable of describing the map between initial and final state distributions.¹⁷

From a practical perspective the most useful model is a state-to-distribution (STD) model from which final state distributions $P(E'_{\text{trans}})$, $P(v')$, and $P(j')$ can be determined for every

initial state (E_{trans}, v, j) . This is what is required for more coarse-grained simulations, such as DSMC. The present work presents state-to-distribution models for the $\text{N}(^4\text{S}) + \text{O}_2(\text{X}^3\Sigma_g^-) \rightarrow \text{NO}(\text{X}^2\Pi) + \text{O}(^3\text{P})$ reaction based on translational energy E_{trans} (instead of the diatom’s internal energy E_{int} , see Ref.¹⁸) and final vibrational state assignment including mechanical ro-vibrational coupling. It has been suspected earlier¹⁸ that including such coupling may benefit model performance for high (v, j) states. The trained ML models are based on data used for the earlier STD model¹⁸ to allow for direct comparison between the different approaches.

The present work is structured as follows. First, the methods used are presented. This is followed by an analysis of the data based on product vibrational state assignments v' using semiclassical mechanics or from a model Hamiltonian (here a truncated Dunham expansion). Then, the performance of NN-trained models based on translational energy together with the two possibilities for assigning final vibrational quantum numbers is assessed and compared. Finally, thermal rates obtained via the two approaches are compared.

Methods

Quasi-Classical Trajectory Simulations and Analysis

The necessary data for ML-based models characterizing atom + diatom collisions are based on quasi-classical trajectory (QCT) simulations. The QCT data and an earlier STD model were used and provided a means to compare the different approaches.¹⁸ Additional QCT simulations were run as needed using the same procedures as discussed before.¹⁸

Initial conditions for QCT simulations were generated from semiclassical quantization.^{19,20} Such an approach couples vibration and rotation in the sense that the initial vibrational

state is assigned from the numerical solution of an integral involving the rotational barrier $j(j+1)/r^2$ where r is the diatomic bond length. After propagation of a specific initial condition (E_{trans}, v, j) for a given impact parameter b , the final states (v', j') for the diatomic need to be determined and the final translational energy E'_{trans} is obtained from the relative velocities and reduced masses of the products. Assigning (v', j') quantum numbers is based on final momenta and positions which are transformed to suitable coordinates. The internal final angular momentum $\mathbf{j}' = \mathbf{q}' \times \mathbf{p}'$ for the product diatomic species is determined from the final position \mathbf{q}' and momentum \mathbf{p}' . Then the quadratic equation

$$j' = -\frac{1}{2} + \frac{1}{2} \left(1 + 4 \frac{\mathbf{j}' \cdot \mathbf{j}'}{\hbar^2} \right)^{\frac{1}{2}} \quad (1)$$

is solved to determine the rotational quantum number (j') as a *non-integer* number.^{19,20}

Using semiclassical (SC) mechanics, the non-integer vibrational quantum number (v') of the final diatomic species is calculated according to^{19,20}

$$v'_{\text{SC}} = -\frac{1}{2} + \frac{1}{\pi \hbar} \int_{r^-}^{r^+} \left\{ 2\mu \left(E_{\text{int}} - V(r) - \frac{\mathbf{j} \cdot \mathbf{j}}{2mr^2} \right) \right\}^{\frac{1}{2}} dr, \quad (2)$$

where r is the diatomic bond length, r^+ and r^- are the turning points of the diatomic species on the effective potential with rotational state j' for internal energy E'_{int} , μ is the reduced mass, and $V(r)$ is the potential energy curve of the product diatom.

Integer ro-vibrational quantum numbers are then assigned as the nearest integers (v', j') using histogram binning. To ensure conservation of total energy, the ro-vibrational energy E'_{int} is recomputed from semiclassical quantization^{19,20} using the integer quantum numbers (v', j') and the final translational energy for the atom+diatom system is adjusted according to $E'_{\text{trans}} = E_{\text{tot}} - E'_{\text{int}}$ where the final total internal energy is determined from the final momenta and positions of the two atoms forming the diatomic.

For high j' quantum numbers the angular momentum causes the potential energy surface of the system to distort, changing the characteristic frequency of the vibrations. A first-order approximation to the energy based on the Dunham expansion is shown in Eq. 3. To include mechanical coupling between vibration and rotation for the products, as afforded by a model Hamiltonian (“MH”), the assignment of the final angular momentum j' is retained as in Eq. 1 but v' is determined from solving

$$\begin{aligned}
 E(v'_{\text{MH}}, j') = & \omega_e(v'_{\text{MH}} + 1/2) - \frac{\omega_e^2}{4D_e}(v'_{\text{MH}} + 1/2)^2 + B_e j'(j' + 1) + D_e[j'(j' + 1)]^2 \\
 & - \alpha_e(v'_{\text{MH}} + 1/2)j'(j' + 1)
 \end{aligned}
 \tag{3}$$

for v' . Here, $E(v', j') = E_{\text{tot}} - E'_{\text{trans}}$, ω_e is the harmonic frequency, $\omega_e x_e$ is the first order correction, B_e is the rotational constant, D_e is the centrifugal constant, and α_e is the ro-vibrational coupling constant. For NO the data is $\omega_e = 1904.20 \text{ cm}^{-1}$, $\omega_e x_e = 14.08 \text{ cm}^{-1}$, $B_e = 1.672 \text{ cm}^{-1}$, $D_e = 0.00000054 \text{ cm}^{-1}$, and $\alpha_e = 0.0171 \text{ cm}^{-1}$.²¹ The corresponding parameters on the MRCI/aug-cc-pVTZ curve for NO are $\omega_e = 1871.0 \text{ cm}^{-1}$ and $\omega_e x_e = 14.04 \text{ cm}^{-1}$.

Neural Network

One approach to creating a model that spans all of the possible probabilities for the outcome of a collision between an atom and a diatom is to use a neural network (NN) representation. Such an approach was used previously in earlier STD work.¹⁸ This NN consists of seven residual layers with two hidden layers per residual layer, and uses 11 input and 254 output nodes corresponding to the 11 features representing the initial reactant state and the 254 amplitudes characterizing the product state distributions. For training, the NN inputs were standardized which ensures that the distributions of the transformed inputs x'_i over

the entire training data are each characterized by $(\bar{x}'_i = 0, \sigma'_i = 1)$. The NN outputs were normalized which ensures that the distributions of the transformed outputs x'_i over the entire training data being characterized by $(\bar{x}'_i = \bar{x}_i, \sigma'_i = 1)$. Standardization of the data generally yields a faster convergence.²² The loss function was the root-mean-squared deviation between reference QCT data and model predictions. As the NN outputs are probabilities, being non-negative even after normalization, a softplus function is used as an activation function of the output layer.

The weights and biases of the NN were initialized according to the Glorot scheme²³ and optimized using Adam²⁴ with an exponentially decaying learning rate. The NN was trained using TensorFlow²⁵ and the set of weights and biases resulting in the smallest loss as evaluated on the validation set were subsequently used for predictions. Overall, final state distributions from 2184 initial conditions on a grid defined by $(0.5 \leq E_{\text{trans}} \leq 5.0)$ eV with $\Delta E_{\text{trans}} = 0.5$ eV $(5.0 \leq E_{\text{trans}} \leq 8.0)$ eV with $\Delta E_{\text{trans}} = 1.0$ eV, $v = [0, 2, 4, 6, 8, 10, 12, 15, 18, 21, 24, 27, 30, 34, 38]$, and $0 \leq j \leq 225$ with step size $\Delta j = 15$ were generated, of which 7 were excluded due to low reaction probability. This “on-grid” set of size $N = 2184$, of which 7 data points were excluded due to low reaction probability, was randomly split into $N_{\text{train}} = 1700$ for training, $N_{\text{valid}} = 400$ for validation, and $N_{\text{test}} = 77$ for testing.¹⁸ The “on-grid” set used for training, validation and test is distinguished from “off-grid” data which refers to initial conditions for which at least one of the entries in (E_{trans}, v, j) differs from an “on-grid” initial condition. All NNs in this work were trained on a 3.60 GHz X 8 Intel Core i7-9700K CPU resulting in training times shorter than 3 minutes. For additional technical details, see Ref.¹⁸

Results

Data Preparation

A first important task in designing a ML model is the selection and preparation of the data. Among other aspects, the present work assesses whether a reliable and predictive STD model can be conceived from training on / predicting of a) the translational energy E'_{trans} and b) the final vibrational quantum number v'_{MH} determined from a model Hamiltonian. The reason for this is that E'_{trans} contains independent physical information from (v', j') states about the collision system whereas E'_{int} and the (v', j') states, as used in the previous model,¹⁸ are somewhat redundant. Similarly, while assignment of v' from semiclassical quantization is one possibility, such an approach neglects part of the mechanical (v, j) coupling. Furthermore, using a model Hamiltonian (such as a Dunham expansion²⁶ or a Watson Hamiltonian,²⁷ based on coefficients fit to represent spectroscopically measured line positions or transitions) for computing v'_{MH} includes valuable information from experiment and makes the model somewhat less dependent on the level of theory at which the intermolecular interactions have been / can be determined in practice. This is the reason to explore changes in the final vibrational distribution if a model Hamiltonian (here the Dunham expression up to first order in coupling vibration and rotation) is used. Retaining higher order terms is also possible to further refine the approach but is not expected to fundamentally change the findings.

E'_{int} versus E'_{trans} : The reason to employ E'_{int} for training the original STD model¹⁸ was that the number of grid points required to faithfully represent $P(E'_{\text{int}})$ was smaller than for $P(E'_{\text{trans}})$ due to the smaller span of energies and smoother features. Figures 1A and B report $P(E'_{\text{trans}})$ and $P(E'_{\text{int}})$ for all 2184 initial reactant conditions (“on-grid”) considered. It appears that $P(E'_{\text{trans}})$ extends to higher energies than $P(E'_{\text{int}})$. This is illustrated by considering a few select final state distributions, see panels E and F in Figure 1.

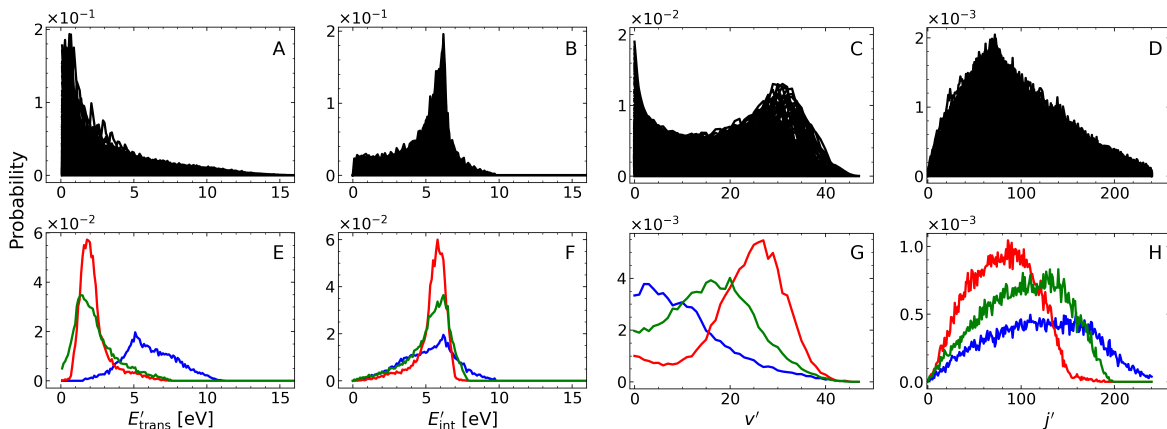


Figure 1: Final state distributions $P(E'_{\text{trans}})$ (panel A), $P(E'_{\text{int}})$ (panel B) $P(v')$ (panel C) and $P(j')$ (panel D) from semiclassical quantization for NO_2 from QCT simulations for all 2184 initial reactant states. Panels E to H report selected distributions $P(E'_{\text{trans}})$, $P(E'_{\text{int}})$, $P(v')$, and $P(j')$ to highlight their different shapes.

Vibrational Quantum Number from Semiclassical Assignment and Ro-vibrational Energy Expression: Final state distributions $P(v')$ and $P(j')$ from using semiclassical quantization in the final state analysis are reported in Figure 1. Panels C and D show product state distributions corresponding to all 2184 initial reactant states considered. For $P(v')$ they are found to extend out to $v' \leq 45$ whereas for $P(j')$ the highest final state is $j' \sim 240$ with maximum values $v'_{\text{max}} = 47$, $j'_{\text{max}} = 240$. Figures 1G and H show individual final state distributions and highlight the various shapes of these distributions encountered depending on the initial condition.

Next, the distributions from using SC and MH final states v'_{SC} and v'_{MH} are presented for all initial conditions, see Figure 2A. The black symbols denote $P(v'_{\text{SC}})$ and extend up to $v'_{\text{SC}} = 46$. This compares with a final state distribution $P(v'_{\text{MH}})$ from using the mechanically coupled energy expression for the assignment of the final state (red symbols) which only extends up to $v'_{\text{MH}} = 36$. The difference (green) between the two assignment schemes is reported in Figure 2B. For $v' \leq 20$ the difference in the population is $\sim 10\%$ which increases to considerably higher values for $v' \sim 30$ and above.

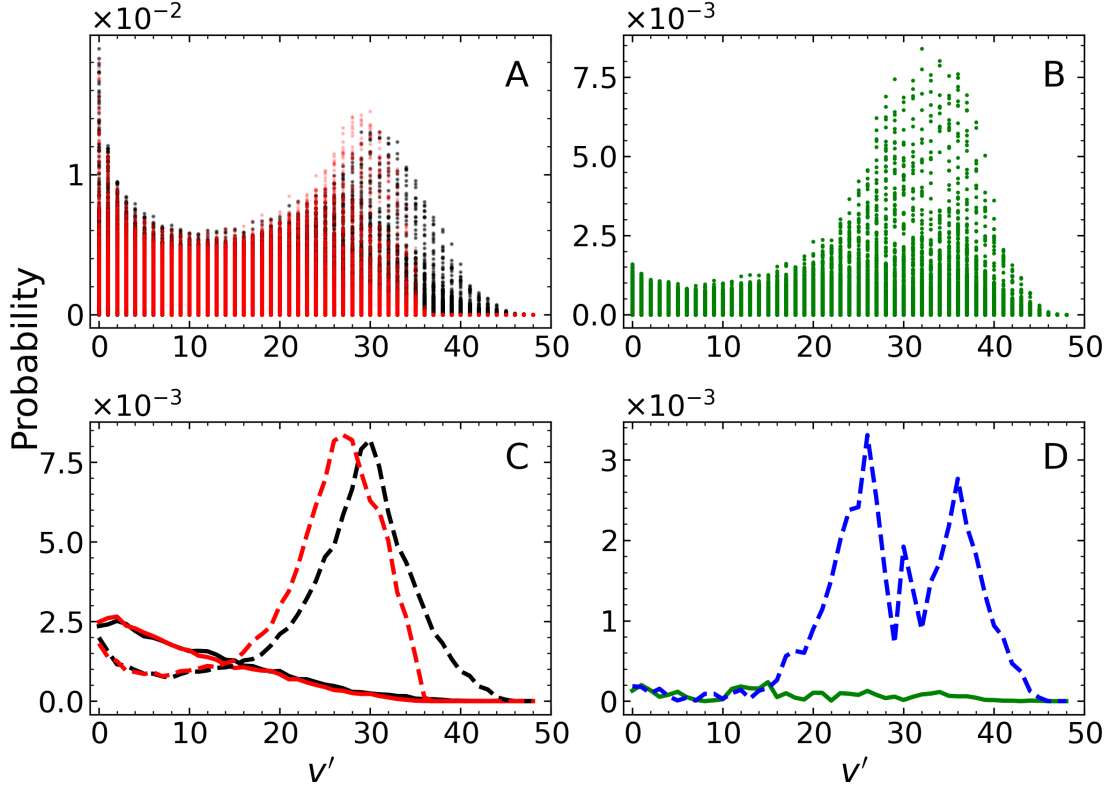


Figure 2: Complete distribution for $P(v'_{SC})$ (black) and $P(v'_{MH})$ (red) for the set of 2184 initial conditions (Panel A) and for selected individual contributions (Panel C). The absolute difference between $P(v'_{SC})$ and $P(v'_{MH})$ is given in panels B (for complete set) & D (for selected individual distributions). Selected test initial conditions: $E_{\text{trans}} = 8.0, v = 0, j = 0$ (solid lines) and $E_{\text{trans}} = 1.0, v = 30, j = 0$ (dashed lines).

Panels C and D of Figure 2 compare final state distributions $P(v'_{SC})$ and $P(v'_{MH})$ for two specific initial states. For $E_{\text{trans}} = 8.0, v = 0, j = 0$ (solid lines) the two final vibrational state distributions are almost indistinguishable, see also their absolute difference (green) in Figure 2D. On the other hand, for initial $E_{\text{trans}} = 1.0, v = 30, j = 0$ (dashed lines) the maximum for $P(v'_{SC})$ (black) is at $v'_{SC} = 30$ which shifts to $v'_{MH} = 26$ for $P(v'_{MH})$. Evidently, the two distributions also differ, see blue dashed line in Figure 2D. The general finding is that including mechanical ro-vibrational coupling in assigning the final vibrational state v'_{MH} populates lower states compared with an analysis based on a semiclassical approach.

Assignment of the final state to integer values (v'_{MH}, j') leads to differences in the corresponding internal energy $E'_{\text{int}}(v'_{\text{MH}}, j')$ from the value obtained when considering $E'_{\text{int}} = E_{\text{tot}} - E'_{\text{trans}}$ based on energy conservation. Hence, the difference $E'_{\text{int}}(v'_{\text{MH}}, j') - E'_{\text{int}}$ has to be redistributed into E'_{trans} which leads to $E'_{\text{trans,MH}}$ from including mechanical coupling in the rovibrational energy. Figure 3A compares the final translational energy distributions $P(E'_{\text{trans,SC}})$ (black) and $P(E'_{\text{trans,MH}})$ (red). The overall shapes of the two distributions are comparable but when considering the absolute difference between the two distributions (Figure 3B, green) variations up to 50 % are found. For high translational energy the absolute differences decay to zero.

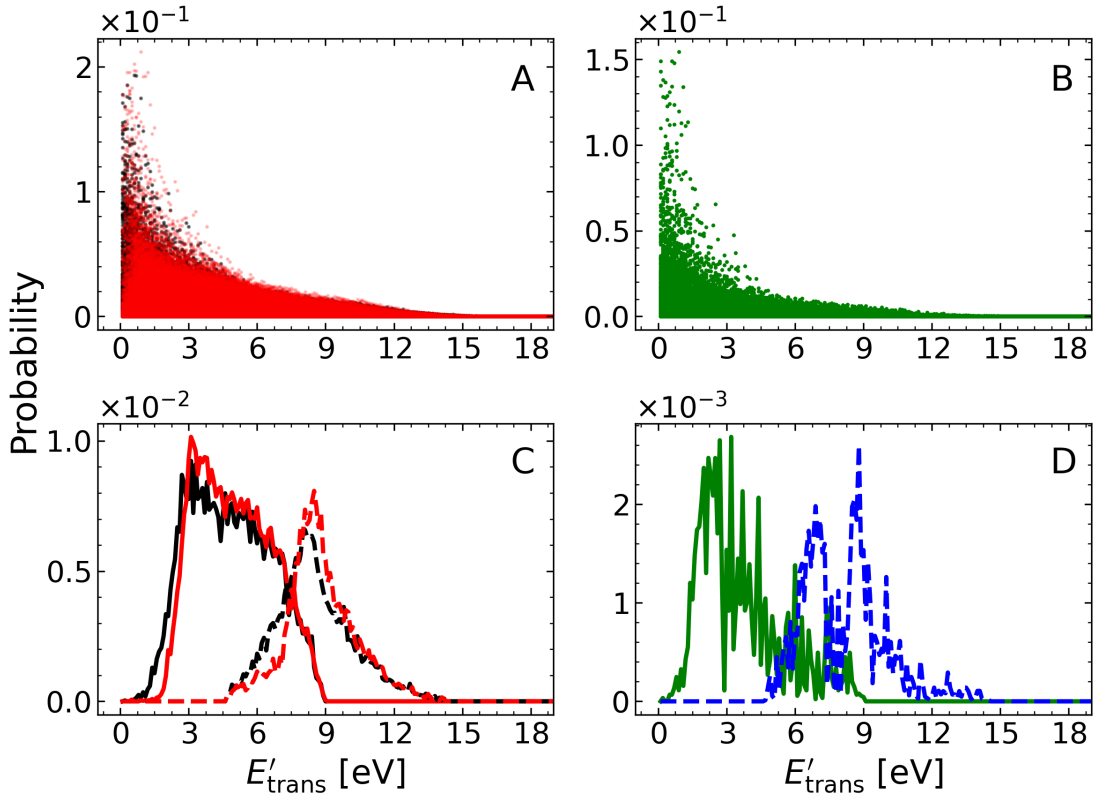


Figure 3: Complete distribution for $P(E'_{\text{trans,SC}})$ (black) and $P(E'_{\text{trans,MH}})$ (red) for the set of 2184 initial conditions (Panel A) and for selected individual contributions (Panel C). The absolute difference between $P(E'_{\text{trans,SC}})$ and $P(E'_{\text{trans,MH}})$ is given in panels B (for complete set) & D (for selected individual distributions) for initial conditions $E_{\text{trans}} = 8.0, v = 0, j = 0$ (solid lines) and $E_{\text{trans}} = 8.0, v = 24, j = 120$ (dashed lines).

Focussing on two specific initial conditions ($E_{\text{trans}} = 8.0, v = 0, j = 0$ and $E_{\text{trans}} = 8.0, v = 24, j = 120$, see Figure 3C) indicate that the overall shapes of the final translational energy distributions depend little on whether mechanical coupling was included or not to determine v' . For initial ($E_{\text{trans}} = 8.0, v = 0, j = 0$) nonzero probability at low translational energy starts at a higher value for an analysis based on MH (red) compared with SC (black). A similar behaviour is seen for the initial condition given by ($E_{\text{trans}} = 8.0, v = 24, j = 120$) (dashed lines in Figure 3C). Absolute differences are reported in Figure 3D and reach a maximum of $\sim 20\%$.

Trained STD Models

Next, full STD models were trained based on assignment of the final vibrational state from semiclassical analysis (v'_{SC}) or using a first-order Dunham expansion (v'_{MH}) together with E_{trans} , respectively. In the following, “on-grid” values refer to initial conditions that were used for training the NN (training, validation, test data - see Methods) and “off-grid” corresponds to initial conditions that differed from “on-grid” values in at least one of the initial conditions (E_{trans}, v, j).

The performance of the trained models in terms of R^2 and RMSD is summarized in Tables 1 and 2. The analysis is carried out for all on-grid-values, excluding seven distributions with low probabilities ($P(v') < 0.005$), and excluding the lowest translational energy $E_{\text{trans}} = 0.5$ eV because the number of QCT simulations may be insufficient to fully converge these final state distributions. In addition, this analysis was also carried out for initial conditions off-grid in (v, j) and at fixed $E_{\text{trans}} = 4.0$ eV. For all degrees of freedom and all test sets $R^2 > 0.97$ which indicates reliable statistical models. Such R^2 measures are also comparable to the performance if instead of using E_{trans} the models are trained on E_{int} for which $R^2 > 0.98$ was found.¹⁸ If simulations at the lowest translational energy (0.5 eV) are ex-

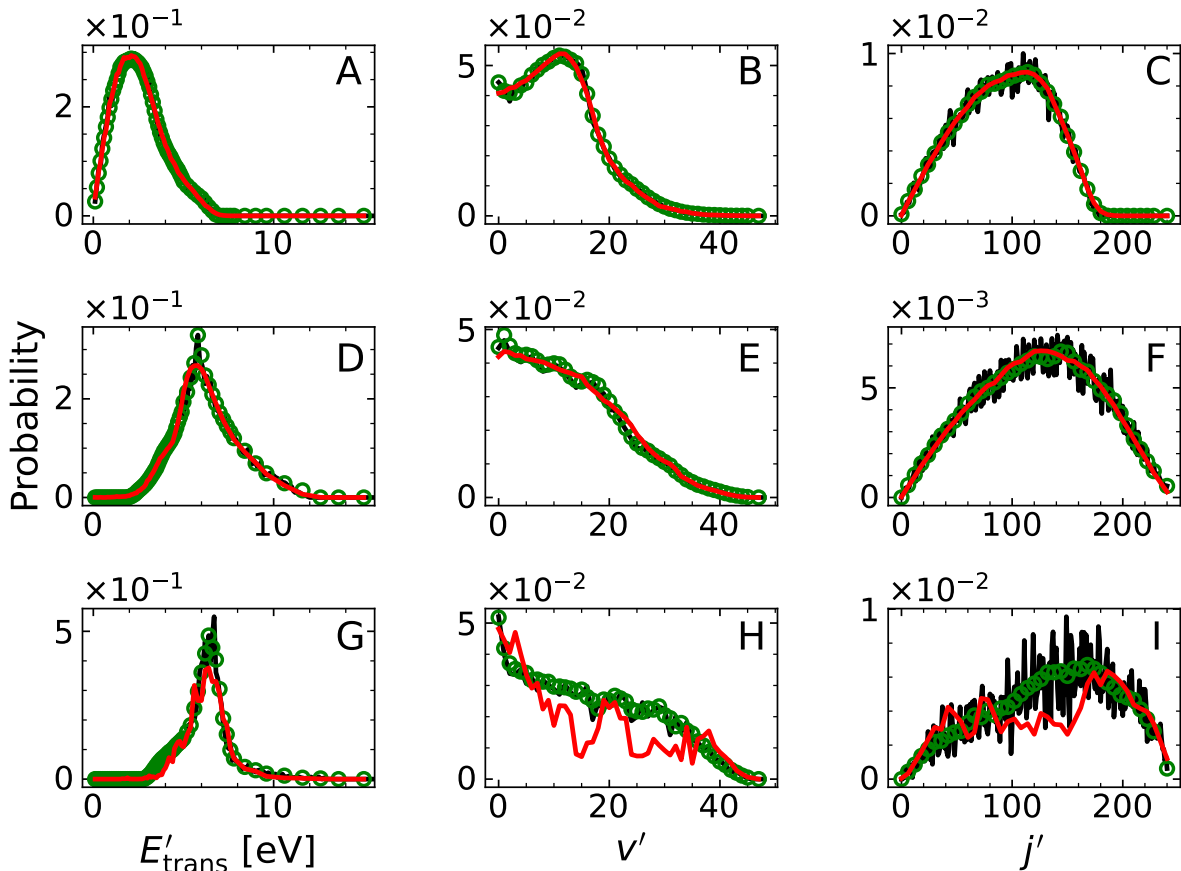


Figure 4: Comparison of product state distributions from QCT (symbols) and STD model evaluation (red solid line) for SC, for initial conditions from the “on-grid” set (excluding $E_{\text{trans}} = 0.5$ eV). STD predictions are for the initial condition for which the prediction is best (top, largest R^2), is closest to the average R^2 (middle), and worst (bottom, lowest R^2), respectively. The corresponding R^2 values for $(P(E'_{\text{trans}}), P(v'), P(j'))$ are: $[0.9985, 0.9985, 0.9995]$ (best); $[0.9880, 0.9954, 0.9895]$ (closest to mean) and $[0.9307, 0.4082, 0.3578]$ (worst). The corresponding reaction probabilities $P_r = N_r/N_{\text{tot}}$ are 0.378, 0.217, and 0.064 for the best, average and worst prediction, respectively. Here, N_{tot} and N_r the total number and number of reactive trajectories, respectively.

cluded, the performance is somewhat improved for all degrees of freedom. Finally, whether the final vibrational state v' was assigned from a semiclassical treatment or a mechanically coupled energy expression has negligible influence on the performance of the models. When using the RMSD as the measure to compare reference distributions with predictions from the trained STD models (see Table 2) similar conclusions are drawn as for R^2 .

Table 1: R^2 between QCT results and the trained STD model based on E_{trans} and either semiclassical or mechanically coupled determination of v' . On-grid (All) is for all initial conditions from the training, validation and test set for all translational energies considered. The numbers in bracket are from the test set (77 initial conditions) only. On-grid* and Off-grid* are for initial conditions with $E_{\text{trans}} = 4.0$ eV only and Off-grid* contains all initial conditions for which either v , j , or both (v, j) differed from the values used for the training, validation and test sets.

	On-grid (All)	On-grid (test)	On-grid*	Off-grid*
$P(E'_{\text{trans,SC}})$	0.9878	0.9844	0.9949	0.9918
$P(E'_{\text{trans,MH}})$	0.9737	0.9840	0.9959	0.9942
$P(v'_{\text{SC}})$	0.9881	0.9835	0.9949	0.9961
$P(v'_{\text{MH}})$	0.9834	0.9817	0.9966	0.9972
$P(j'_{\text{SC}})$	0.9845	0.9816	0.9940	0.9950
$P(j'_{\text{MH}})$	0.9879	0.9882	0.9950	0.9951
“SC” (overall)	0.9868	0.9832	0.9946	0.9943
“MH” (overall)	0.9817	0.9846	0.9959	0.9955

An explicit comparison of final state distributions from models based on SC (Figure 4) and MH (Figure 5) for assigning the final vibrational state is provided for the best-performing, for an average-performing, and for the least performing distribution. The QCT final state distributions are shown as green open circle and the STD predictions as the red solid line. For the best-performing prediction the STD model closely follows the target data. This is still the case for a prediction that represents an average performance. It is also notable that the shape of the distributions for the same degree of freedom can change appreciably, depending on the initial condition. For the worst-performing prediction it is found that SC (see Figure 4) leads to a visually inferior model compared to using MH (Figure 5). In both worst-performing cases, the number of reactive trajectories N_r as a fraction of the total number of trajectories N_{tot} is only $\sim 5\%$ and increasing the sampling may also lead to better reference data.

For a more global characterization of the final states for the entire range of possible initial

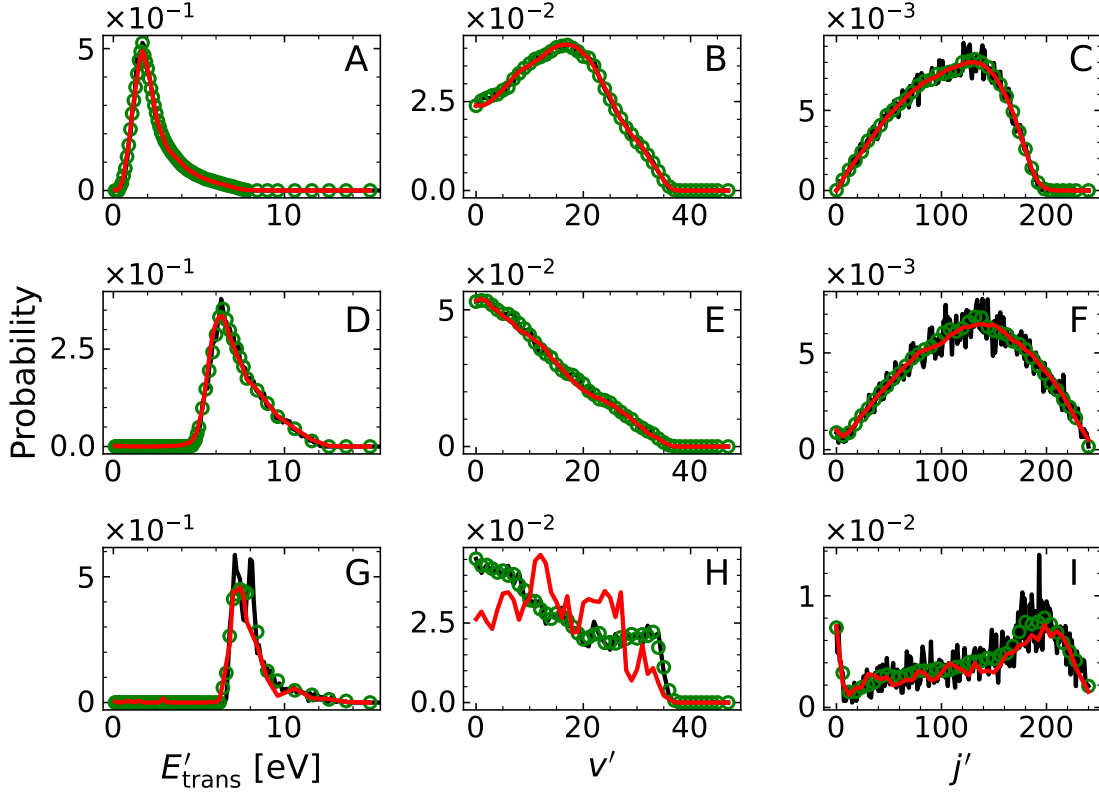


Figure 5: Comparison of product state distributions from QCT (symbols) and STD model evaluation (red solid line) for MH, for initial conditions from the “on-grid” set (excluding $E_{\text{trans}} = 0.5$ eV). STD predictions are for the initial condition for which the prediction is best (top, largest R^2), is closest to the average R^2 (middle), and worst (bottom, lowest R^2), respectively. The corresponding R^2 for $(P(E'_{\text{trans}}), P(v'), P(j'))$ are: $[0.9987, 0.9987, 0.9991]$ (best); $[0.9911, 0.9971, 0.9911]$ (closest to mean) and $[0.9741, 0.5043, 0.8305]$ (worst). The corresponding reaction probabilities $P_r = N_r/N_{\text{tot}}$ are 0.365, 0.308, and 0.044 for the best, average and worst prediction, respectively. Here, N_{tot} and N_r the total number and number of reactive trajectories, respectively.

states (v, j) , 5 independent models were trained from reference data for SC (Figure 6A) and MH (Figure 6B). The averaged R^2 over all 5 models using “on-grid” (see Methods; black circles) and “off-grid” (see caption Figure 6; crosses) data for each of the initial states considered shows a uniformly high performance for both approaches with typical $R^2 \sim 0.98$ or better. For the highest v -values the absolute difference between using MH and SC expressions for v' becomes most apparent. There, using a “MH” model appears to slightly outperform an analysis based on a “SC” energy expression. But the differences are insignificant.

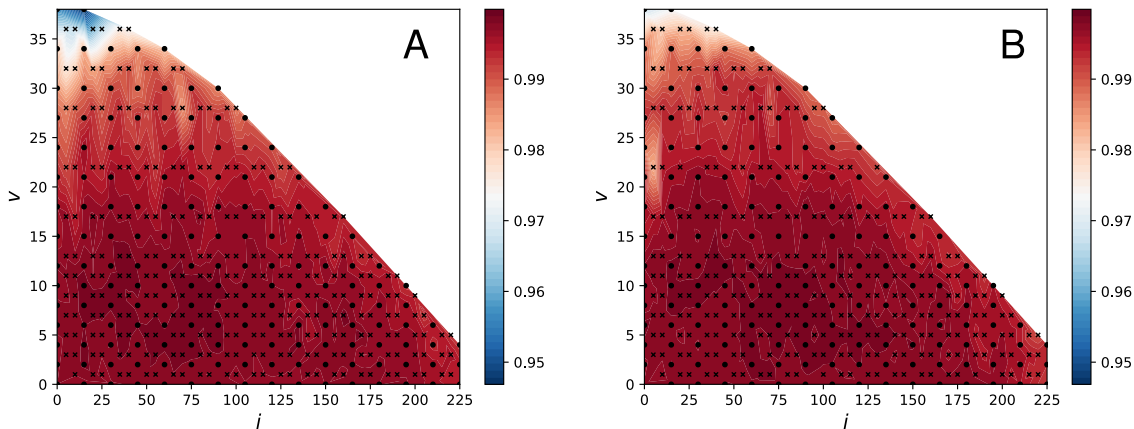


Figure 6: 2D map of the averaged (over 5 independently trained STD models) R^2 values between QCT data ($P(E'_{\text{trans}}), P(v'), P(j')$) and STD evaluation for initial conditions “on-grid” (see Methods, circles) and “off-grid” ($[v = 1, 3, 5, 7, 9, 11, 13, 17, 22, 28, 32, 36]$, $j = [10, 20, 25, 35, 40, 50, 55, 65, 70, 80, 85, 100, 110, 115, 125, 130, 140, 145, 155, 160, 170, 175, 185, 200, 205, 215, 220]$, crosses). Panel A for “SC” and panel B for “MH” assignment of the final vibrational state. All QCT simulations were carried out at $E_{\text{trans}} = 4.0$ eV.

Thermal Rates

It is also of interest to determine thermal rates from the trained models. In general, such a rate is determined from the reaction probability P_r according to

$$k(T) = g(T) \sqrt{\frac{8k_B T}{\pi \mu}} \pi b_{\text{max}}^2 P_r. \quad (4)$$

For QCT simulations based on stratified sampling of the impact parameter b , $P_r = \sum_{k=1}^K V_k \frac{N_k^r}{N_k^{\text{tot}}}$ where N_k^r and N_k^{tot} are the number of reactive and total trajectories, respectively, for stratum k with impact parameter b_k . The fractional volumes $V_k = \frac{b_k^2 - b_{k-1}^2}{b_{\text{max}}^2}$ of stratum k obey $\sum_{k=1}^K V_k = 1$. For the STD model the reaction probability can be obtained as $P_r = \int_{E=0}^{E_{\text{max}}} P(E) dE$ where $E = E'_{\text{trans}}$ and $E_{\text{max}} = 15.0$ eV. For the forward $\text{N}(^4\text{S}) + \text{O}_2(\text{X}^3\Sigma_g^-) \rightarrow \text{NO}(\text{X}^2\Pi) + \text{O}(^3\text{P})$ reaction in the $^4\text{A}'$ electronic state the degeneracy factor $g(T) = 1/3$ and μ is the reduced mass of the reactants.²⁸ The two approaches are compared

in Figure 7 and favourable agreement is found over a wide temperature range. Hence, the STD model can also be used to determine macroscopic quantities such as realistic reaction rates which is essential.

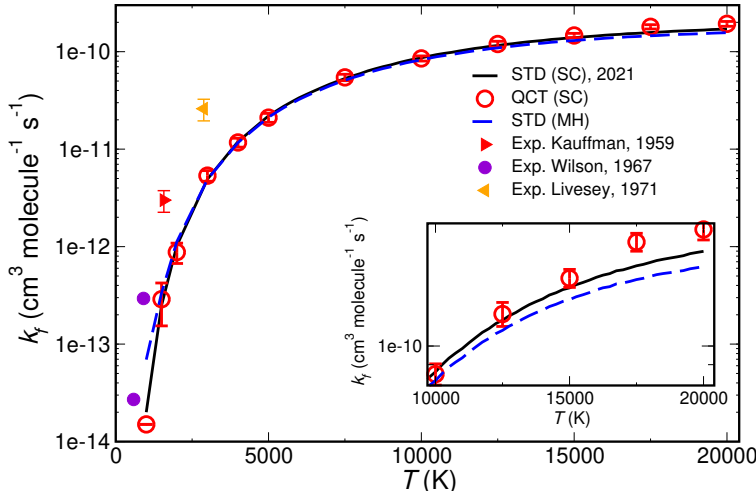


Figure 7: The thermal forward rate k_f calculated from QCT (open red circle) and STD model (solid black line) for the $^4A'$ state of the $\text{N}(^4\text{S}) + \text{O}_2(\text{X}^3\Sigma_g^-) \rightarrow \text{NO}(\text{X}^2\Pi) + \text{O}(^3\text{P})$ reaction between 1000 and 20000 K. Additional simulations were made with the STD model based on E_{trans} and “MH” (blue dashed line). The present rates agree quantitatively with those directly obtained from QCT simulations, in particular considering the reduction of required compute time by 7 orders of magnitude or more. Rates for “MH” are expected to change slightly if higher-order terms in the Dunham expansion are included. Experimental total forward reaction rate k_f (including contributions from the doublet and the quartet states) are also shown for comparison: (red triangle),²⁹ (orange triangle)³⁰ and (magenta circle).³¹

Discussion and Conclusion

The present work discusses a rapid, accurate, and physics-based model to determine final state distributions for given initial conditions (E_{trans}, v, j) for atom+diatom reactions. It is shown that training on E'_{trans} and v' from an energy expression including mechanical coupling (Dunham expression) yields a model performance of $R^2 \sim 0.98$ or better compared with rigorous QCT reference simulations. Models based on (E_{trans}, v, j) are more physically

meaningful than those using (E_{int}, v, j) because E_{int} and (v, j) are partly redundant whereas E_{trans} contains new, complementary, and physically relevant information. The gain in speed compared to explicit QCT simulations is about 7 orders of magnitude required for inference (i.e., excluding training the NN which is minutes, and generating the required QCT reference data for training) assuming that 10^5 QCT trajectories are sufficient for converged final state distributions. Hence, this is a promising avenue to be used in more coarse-grained simulations of reaction networks relevant to hypersonics and combustion.

Including coupling in determining the final v' state of the diatomic by means of a truncated Dunham expansion as a typical model Hamiltonian (MH) leads to population of lower v' states than assignment from semiclassical mechanics (SC). The overall shapes of the final state distributions $P(v'_{\text{SC}})$ and $P(v'_{\text{MH}})$ do not change appreciably, see for example Figure 2. However, final vibrational distributions from SC extend to higher values v' than those from using a Dunham expansion. The influence of this effect is illustrated in Figure 8 which compares final internal energy distributions from the two assignment schemes (SC and MH) for all on-grid initial conditions. The relevant NO dissociation energies from the SC and MH models are also indicated and allow to determine the fraction of final states that are above this threshold to be 21 % and 14 %, respectively, for SC and MH.

If larger products than diatomics are produced in such reactions, it is expected that the MH approach for assigning final vibrational states is more convenient than an assignment based on semiclassical mechanics. Furthermore, using effective Hamiltonians to determine internal final states of molecular fragments opens the possibility to blend accurate spectroscopic information into such models which makes them less dependent on the level of quantum chemical theory at which the intermolecular interactions can be practically described. For example, multi-reference configuration interaction (MRCI) calculations with extended basis sets (triple zeta and larger) for molecules with more than 3 atoms can quickly become

computationally prohibitive. However, it should also be noted that both schemes have their advantages and drawbacks. For experimental observables, such as thermal rates, both models perform on par, see Figure 7.

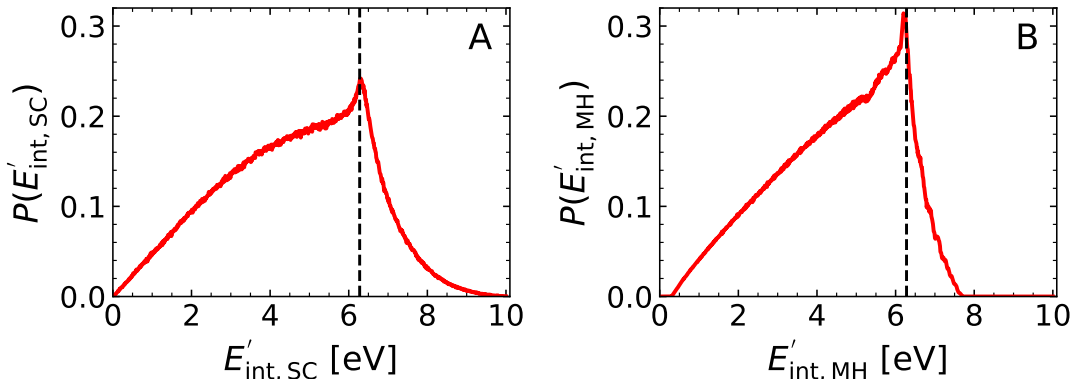


Figure 8: Final internal energy distribution $P(E'_{\text{int}})$ depending on the assignment scheme (SC, MH) used. Distributions are generated from the complete data set (on-grid and off-grid) used as initial conditions in the QCT simulations. The dissociation energy for NO (dashed black) is shown as well (6.27 eV and 6.29 eV for SC and MH, respectively, compared with 6.50 eV from experiment.²¹) and the percentage of population above dissociation is 21 % and 14 % for SC and MH, respectively. The D_e value for MH was determined from using a scaling factor between experimental D_e , and $D_e = \omega_e^2/(4\omega_e x_e)$ using spectroscopic constants.²¹

The actual population of highly excited states in the product diatom is particularly relevant for hypersonics because such states can easily dissociate during the next collision and the ensuing products (free atoms at high translational energy) induce rich chemistry. In general, highly vibrationally excited states are correlated with facile dissociation whereas high j -values prevent and delay breakup of the diatomic. Furthermore, the vibrational coordinate can also lead to electronic state relaxation rate differences in subsequent reactions.³² Hence, overall, depending on the assignment scheme used for (v, j) the energy partitioning into other degrees of freedom (translation, electronic) will be affected, too.

In summary, the present work demonstrates that it is possible to construct machine-learned

models for final state distributions given state-specific information for the reactants for atom + diatom reactions. The trained models are accurate, rapid to evaluate, and can be extended as needed for other applications, e.g. combustion, by supplying suitable training data. It is anticipated that such approaches are beneficial to perform more coarse-grained modeling to applications in hypersonic flow and computational combustion studies.

Data and Code Availability

Exemplary data sets and code for training and evaluating STD models can be found at <https://github.com/MMunibas/STDMH>.

Supporting Information

The supporting information contains one additional Table.

Acknowledgments

This work was supported by AFOSR, the Swiss National Science Foundation through grants 200021-117810, 200020-188724, the NCCR MUST, and the University of Basel (to MM). J.A. acknowledges financial support from the Swiss National Science Foundation individual grant (Grant No. 200020_200481). Discussions with Dr. D. Koner are greatly appreciated.

References

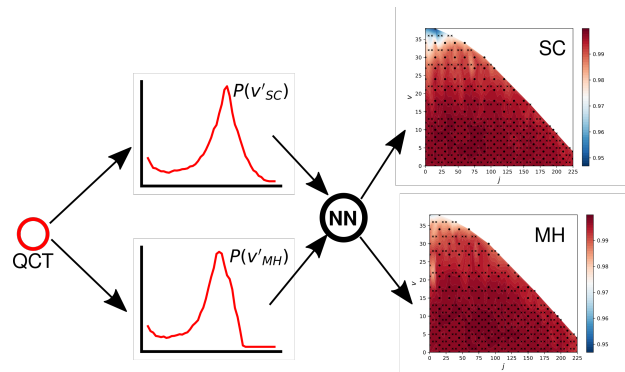
- (1) Knight, D.; Longo, J.; Drikakis, D.; Gaitonde, D.; Lani, A.; Nompelis, I.; Reimann, B.; Walpot, L. Assessment of CFD capability for prediction of hypersonic shock interactions. *Progr. Aerospace Sci.* **2012**, *48-49*, 8–26.

- (2) Boyd, I. D.; Schwartzentruber, T. E. *Nonequilibrium Gas Dynamics and Molecular Simulation*; Cambridge University Press, New York, 2017.
- (3) Boyd, I. D. Computation of hypersonic flows using the direct simulation Monte Carlo method. *J. Spacecr. Rockets* **2015**, *52*, 38–53.
- (4) Bird, G. A. *Molecular Gas Dynamics and the Direct Simulation of Gas Flows*; 1994.
- (5) Boyd, I.; Bose, D.; Candler, G. Monte Carlo modeling of nitric oxide formation based on quasi-classical trajectory calculations. *Phys. Fluids* **1997**, *9*, 1162–1170.
- (6) Park, C. Review of Chemical-Kinetic Problems of Future NASA Missions. 1. Earth Entries. *J. Thermophys. Heat Transf.* **1993**, *7*, 385–398.
- (7) Park, C.; Jaffe, R.; Partridge, H. Chemical-kinetic parameters of hyperbolic Earth entry. *J. Thermophys. Heat Transf.* **2001**, *15*, 76–90.
- (8) Millikan, R. C.; White, D. R. Systematics of Vibrational Relaxation. *J. Chem. Phys.* **1963**, *39*, 3209–3213.
- (9) Park, C.; Howe, J. T.; Jaffe, R. L.; Candler, G. V. Review of chemical-kinetic problems of future NASA missions. II-Mars entries. *J. Thermophys. Heat Transf.* **1994**, *8*, 9–23.
- (10) Landau, L. Theory of sound dispersion. *Physikalische zeitschrift der Sowjetunion* **1936**, *10*, 34–43.
- (11) Nikitin, E.; Troe, J. 70 years of Landau–Teller theory for collisional energy transfer. Semiclassical three-dimensional generalizations of the classical collinear model. *Phys. Chem. Chem. Phys.* **2008**, *10*, 1483–1501.
- (12) Singh, N.; Schwartzentruber, T. Non-Boltzmann vibrational energy distributions and coupling to dissociation rate. *J. Chem. Phys.* **2020**, *152*, 224301.

- (13) Singh, N.; Schwartzentruber, T. Consistent kinetic–continuum dissociation model I. Kinetic formulation. *J. Chem. Phys.* **2020**, *152*, 224302.
- (14) Marrone, P. V.; Treanor, C. E. Chemical relaxation with preferential dissociation from excited vibrational levels. *Phys. Fluids* **1963**, *6*, 1215–1221.
- (15) Valentini, P.; Schwartzentruber, T. E.; Bender, J. D.; Candler, G. V. Dynamics of nitrogen dissociation from direct molecular simulation. *Phys. Rev. Fluids* **2016**, *1*.
- (16) Koner, D.; Unke, O. T.; Boe, K.; Bemish, R. J.; Meuwly, M. Exhaustive state-to-state cross sections for reactive molecular collisions from importance sampling simulation and a neural network representation. *J. Chem. Phys.* **2019**, *150*, 211101.
- (17) Arnold, J.; Koner, D.; Käser, S.; Singh, N.; Bemish, R. J.; Meuwly, M. Machine Learning for Observables: Reactant to Product State Distributions for Atom-Diatom Collisions. *J. Phys. Chem. A* **2020**, *124*, 7177–7190.
- (18) Arnold, J.; San Vicente Veliz, J. C.; Koner, D.; Singh, N.; Bemish, R. J.; Meuwly, M. Machine learning product state distributions from initial reactant states for a reactive atom–diatom collision system. *J. Chem. Phys.* **2022**, *156*, 034301.
- (19) Karplus, M.; Porter, R. N.; Sharma, R. D. Exchange Reactions with Activation Energy. I. Simple Barrier Potential for (H, H₂). *J. Chem. Phys.* **1965**, *43*, 3259–3287.
- (20) Truhlar, D. G.; Muckerman, J. T. In *Atom - Molecule Collision Theory*; Bernstein, R. B., Ed.; Springer US, 1979; pp 505–566.
- (21) Herzberg, G. *Molecular spectra and molecular structure: Spectra of diatomic molecules*; Van Nostrand Reinhold, New York, 1950.
- (22) LeCun, Y. A.; Bottou, L.; Orr, G. B.; Müller, K.-R. *Neural networks: Tricks of the trade*; Springer, 2012; Vol. 7700; p 948.

- (23) Glorot, X.; Bengio, Y. Understanding the difficulty of training deep feedforward neural networks. Proceedings of the 13th International Conference on Artificial Intelligence and Statistics. 2010; pp 249–256.
- (24) Kingma, D.; Ba, J. Adam: A method for stochastic optimization. *arXiv preprint arXiv:1412.6980* **2014**,
- (25) Abadi, M. et al. Tensorflow: Large-scale machine learning on heterogeneous distributed systems. *arXiv preprint arXiv:1603.04467* **2016**,
- (26) Dunham, J. The Wentzel-Brillouin-Kramers method of solving the wave equation. *Phys. Rep.* **1932**, *41*, 713.
- (27) Watson, J. K. Simplification of the molecular vibration-rotation Hamiltonian. *Mol. Phys.* **1968**, *15*, 479–490.
- (28) San Vicente Veliz, J. C.; Koner, D.; Schwilk, M.; Bemish, R. J.; Meuwly, M. The N(⁴S) + O₂(X ³Σ_g⁻) ↔ O(³P) + NO(X ²Π) reaction: thermal and vibrational relaxation rates for the ²A', ⁴A' and ²A'' states. *Phys. Chem. Chem. Phys.* **2020**, *22*, 3927–3939.
- (29) Kaufman, F.; Decker, L. J. *7th Symp. (Int.) Combustion* **1959**, 57.
- (30) Livesey, J. B.; Roberts, A. L.; Williams, A. The Formation of Oxides of Nitrogen in some Oxy-Propane Flames. *Combust. Sci. Technol.* **1971**, *4*, 9–15.
- (31) Wilson, W. Rate constant for the reaction N + O₂ → NO + O. *J. Chem. Phys.* **1967**, *46*, 2017–2018.
- (32) Andrienko, D.; Boyd, I. D. Vibrational relaxation and dissociation in O₂-O mixtures. 46th AIAA Thermophysics Conference. 2016; p 4021.

Table of Contents Graphics



Supporting Information:

Table 2: RMSD between QCT results and the trained STD model based on E_{trans} and either semiclassical or mechanically coupled determination of v' . On-grid (All) is for all initial conditions from the training, validation and test set for all translational energies considered. The numbers in bracket are from the test set (77 initial conditions) only. On-grid* and Off-grid* are for initial conditions with $E_{\text{trans}} = 4.0$ eV only and Off-grid* contains all initial conditions for which either v , j , or both (v, j) differed from the values used for the training, validation and test sets.

	On-grid (All)	On-grid (test)	On-grid*	Off-grid*
$P(E'_{\text{trans,SC}})$	0.0110	0.0134	0.0053	0.0080
$P(E'_{\text{trans,MH}})$	0.0143	0.0151	0.0056	0.0081
$P(v'_{\text{SC}})$	0.0015	0.0019	0.0011	0.0011
$P(v'_{\text{MH}})$	0.0019	0.0025	0.0011	0.0010
$P(j'_{\text{SC}})$	0.0002	0.0003	0.0002	0.0002
$P(j'_{\text{MH}})$	0.0002	0.0003	0.0002	0.0002
“SC” (overall)	0.0042	0.0052	0.0022	0.0031
“MH” (overall)	0.0055	0.0059	0.0028	0.0031